Indirect Combustion Noise: Experimental Investigation of the Vortex Sound Generation in a Choked Convergent-divergent Nozzle

Nancy Kings, Lars Enghardt, Friedrich Bake

ACOUSTICS 2012

Indirect Combustion Noise: Experimental Investigation of the Vortex Sound Generation in a Choked Convergent-divergent Nozzle

N. Kings, L. Enghardt and F. Bake

German Aerospace Center (DLR), Mueller-Breslau-Str. 8, 10623 Berlin, Germany
nancy.kings@dlr.de

Combustion noise in gas turbines consists of direct noise related to the unsteady combustion process itself and indirect noise. As known, indirect noise is produced when entropy fluctuations originating from the combustor are accelerated through the turbine. According to the characterisation of the flow by pressure, entropy and vorticity perturbations accelerated vorticity fluctuations are likewise expected to generate indirect noise. The sound generation mechanism through the acceleration of vorticity fluctuations was studied in a model experiment. Within a swirl free and a swirling tube flow, vorticity fluctuations were generated artificially by injecting temporarily additional air into the mean flow which were convected and accelerated in a choked convergent-divergent nozzle. The produced acoustic waves were detected downstream of the nozzle. In addition, the spatial and temporal changes of the velocity field upstream of the nozzle were determined with Hot-Wire Anemometry measurements. Direct and vortex sound was identified and separated by varying the distance between the air-injection inlet and the nozzle. The intensity of the swirling flow and of the vorticity fluctuation was modified. Increasing the air-injection into the mean flow augments the generated indirect noise.

1 Introduction

In recent years combustion noise has gained in importance as consequence of the achieved noise reduction of other jet engine components. Combustion noise consists of direct noise related to the unsteady combustion process itself and indirect combustion noise. As known, indirect noise is produced when entropy fluctuations originating from the combustor are accelerated through the turbine. According to the characterisation of the flow by pressure, entropy and vorticity perturbations accelerated vorticity fluctuations are likewise expected to generate indirect noise. Further research regarding the indirect noise generation mechanisms is needed to determine its contribution to the indirect or core noise.

In the seventies, one of the first analytical investigations on sound generation caused by convected flow inhomogeneities was published by Morfey [12]. Furthermore, Marble and Candel [10] described the sound generation through entropy waves in nozzle and diffuser flows in a one-dimensional theory which was refined and applied by Cumpsty and Marble [4, 5] to a turbine stage. Cumpsty [3] characterised the generation of pressure, entropy and vorticity perturbations by unsteady combustion or heat addition and compared the amplitudes of direct and entropy noise. The approach of Marble and Candel [10] was extended by Moase et al. [11] with a linear velocity assumption to investigate frequency effects in nozzles and diffusers. Stow et al. [13] studied the reflection of circumferential modes in a choked nozzle by applying a phase correction to the reflection coefficient obtained for the compact case. Research on entropy noise has been done by Bake et al. [1], experimentally as well as numerically. Leyko et al. [12] studied the entropy noise generation in supersonic nozzles applying a numerical and analytical approach. Gho and Morgans [6] analysed the magnitude and phase of the transmitted acoustic response of finite-length nozzles to entropy and acoustic disturbances at the inlet. Concerning the generation of vortex sound a comprehensive theoretical description was given by Howe [7]. Hulshoff et al. [9] examined the sound production of a vortex passing a nozzle using time-accurate inviscid flow computations. Recently, analytical expressions for the sound generation through entropy and vorticity fluctuations with regard to indirect combustion noise were also formulated by Howe [8]. In summary, previous work on this research field was mostly conducted numerically or analytically.

The objective of the work presented here was to study experimentally the sound generation through accelerated vorticity fluctuations. Therefore, a model experiment has been built up. Within a swirl free and a swirling tube flow, vorticity fluctuations were generated artificially by injecting temporarily additional air into the mean flow which were convected and accelerated in a choked convergent-divergent nozzle. During the acceleration of the vorticity fluctuations pressure disturbances are produced propagating up- and downstream as acoustic pressure waves. The generated acoustic waves were detected downstream of the nozzle, and in addition, the spatial and temporal changes of the velocity field upstream of the nozzle were determined with Hot-Wire Anemometry measurements. The time signals of the velocity components and of the downstream propagating acoustic waves were recorded simultaneously.

2 Acoustic Analogy

Analytical expressions were derived by Howe [7],[8] for perturbations due to the convection of entropic and vortical inhomogeneities in duct flows with varying cross sections. Howe reformulated the Lighthill's equation in terms of the total enthalpy B for a homogeneous fluid by taking the momentum equation in Crocco's form (Eq. 1) and the continuity equation (Eq. 2):

$$\frac{\partial \mathbf{v}}{\partial t} + \nabla B = -\boldsymbol{\omega} \times \mathbf{v} + T\nabla s \tag{1}$$

$$\frac{1}{\rho}\frac{D\rho}{Dt} = -\nabla \cdot \mathbf{v} \tag{2}$$

where $\mathbf{v}$ is the velocity vector, s the specific entropy, T the temperature, $\frac{D}{Dt}$ the material derivative, $\boldsymbol{\omega}$ is the vorticity vector, and B the total enthalpy. Multiply (Eq. 1) by the density ρ and take the divergence:

$$\mathrm{div}\left(\rho\frac{\partial \mathbf{v}}{\partial t}\right) + \nabla \cdot (\rho \nabla B) = -\mathrm{div}\,(\rho\boldsymbol{\omega} \times \mathbf{v} - \rho T \nabla s) \tag{3}$$

Using (Eq. 2) the first term $\left(\mathrm{div}\left(\rho\frac{\partial \mathbf{v}}{\partial t}\right)\right)$ can be replaced in terms of B and considering an isentropic flow with s = const equation (Eq. 3) simplifies to the vortex sound equation:

$$\left\{\frac{D}{Dt}\left(\frac{1}{c^2}\frac{D}{Dt}\right) - \frac{1}{\rho}\nabla \cdot (\rho\nabla)\right\} B = \frac{1}{\rho}\mathrm{div}\,(\rho\boldsymbol{\omega} \times \mathbf{v}) \tag{4}$$

The right-hand side of equation (Eq. 4) emphasises on the vorticity as a sound source. Without vorticity fluctuations the total enthalpy B is constant and no sound waves are generated. With vorticity fluctuations the divergence term accounts for the sound production by vortex motions.

3 Experiment

The Vorticity Wave Generator (VWG) test rig, shown in Figure 1, consists of a straight tube flow supplied by the laboratory compressed-air system. Two versions of Vorticity Wave Generator modules (VWG-Module 1 or 2) can be integrated in the tube to induce vorticity fluctuations within the main flow.

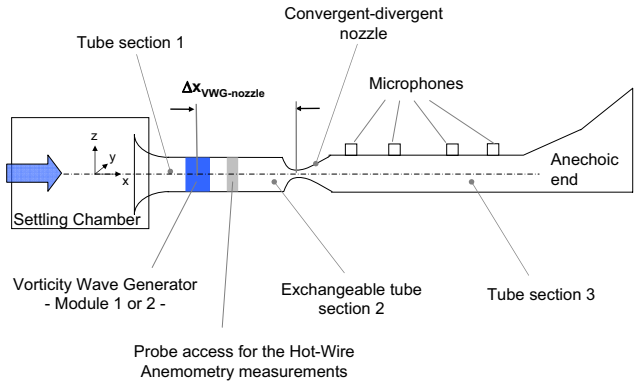

Figure 1: Sketch of the Vorticity Wave Generator.

The components of VWG-Module 1 are the vortex module which is a tube section serving as base body, an injector nozzle, and a fast-switching valve. Two inlets in the base body allow the air-injection via the fast-switching valve into the main flow. Therewith, different vortex structures can be generated by injecting temporarily additional air either in circumferential or in radial direction into the main flow. Applying the circumferential air-injection of VWG-module 1 changes temporarily the swirl free tube flow into a swirling flow for the duration of the valve opening.

VWG-Module 2 consists of the tube section serving as base body, two inlet chambers and a fast-switching valve. This vortex module has eight inlet ports distributed equally around the circumference of the tube. Via four of these inlets in the base body, with 90° angular distance in between, a constant mass flow is added in circumferential direction into the main flow yielding to a steady swirling flow in the tube. The added mass flow through the four inlets is stabilised and equalised by an upstream inlet chamber. The swirl can be changed by varying the axial ($\dot{m}_a$) and the circumferential ($\dot{m}_c$) flow rates in the tube, accordingly the mass flow ratio $\dot{m}_c/\dot{m}_a$ is used as parameter for the swirl intensity. Via the other four inlets temporarily additional air is injected into the mean swirling flow. An upstream inlet chamber secures constant mass flow rates through each of the inlets and simultaneous injection times. Each mass flow rate in the setup is determined by a mass flow controller, this includes the main flow, the temporarily injected mass flow via the fast-switching valve as well as the constant mass flow added in circumferential direction into the main flow.

The main flow enters the setup into a settling chamber with a honeycomb flow straightener, left hand side of Figure 1, and is conducted via a bell mouth intake into the first tube section. Tube section 1 has an inner diameter of 30 mm and is 100 mm in length. The flow passes subsequently either of the two vortex modules where the vorticity fluctuation is induced within the main flow. The access for the Hot-Wire Anemometry measurements is located 50 mm downstream of the vortex module and allows the mounting of one sensor fixing equipped with a hot-wire probe. The used X-wire probes are adjustable in radial and circumferential direction to determine the velocity field over the cross-sectional area of the tube. The tube section 2, after the Hot-Wire Anemometry access, is exchangeable so that different distances between the vortex module and the subsequent nozzle throat can be realised. The following nozzle is convergent-divergent; the convergent part is 13 mm and the divergent 250 mm in length. The Mach number in the nozzle throat of 7.5 mm diameter can be adjusted up to M = 1.0. Downstream of the nozzle the flow passes four wall-flush mounted microphones integrated in tube section 3. The microphone tube section, 1020 mm in length and 40 mm in diameter, is connected to a flexible tube of 980 mm which ends in an adapter section changing from round to square cross section. The flow leaves the test rig through an anechoic termination to minimise acoustic reflections into the measurement section.

The DLR hot-wire measurement system is a Constant-Temperature Anemometer (CTA) and bases on the cooling effect of a flow on a heated wire. In a typical CTA circuit, the sensor is placed in one arm of a Wheatstone bridge and is heated by the electric current. A servo amplifier controls the current to the wire to restore its resistance and hence its temperature. With the amplifier feedback the bridge is kept balanced, independent of the cooling imposed by the flow. The voltage difference across the bridge is a measure of the heat transfer and therewith related to the incident flow velocity. The CTA provides continuous time series of the instantaneous velocity, processable into mean component and fluctuation.

The X-wire probe used as sensor consists of two inclined tungsten wires, each 2.8 mm long and 9μm in diameter. At its ends, each wire is connected to needle-shaped prongs. The inclination angle of the two wires on the X-probe is about 90°. According to the wire orientation the measurement of two velocity components in the tube is possible, either the axial and radial or the axial and circumferential. A comprehensive description of Hot-Wire Anemometry, its principles and signal analysis is given in Bruun [2].

4 Measurement results

The measurements were conducted with both Vorticity Wave Generator Modules with pulsed air-injection into the main flow. Accordingly, the fast-switching valve was opened 100 ms per second controlled by a function generator. In the post processing, microphone and X-wire probe signals were phase-averaged over 300 pulses using the excitation signal as reference. Phase-averaging the raw pressure signals reduces the random noise of the air line upstream as well as the stochastic injector noise emitted permanently during the valve opening duration. In addition, the uncorrelated velocity fluctuations contained in the raw bridge voltage signals are minimised. The phase-averaged data of the hot-wires were transformed into the velocity components using the previously determined calibration coefficients.

4.1 Velocity changes due to air-injection into a swirl free tube flow

The induced velocity changes due to the circumferential air - injection into the swirl free tube flow using VWG-

Module 1 are depicted in Figure 2 and 3. The velocity profile over the tube cross section in z-direction was selected. The nozzle Mach number was adjusted to $M_{nozzle} = 1.0$ and the injected mass flow rate to $\dot{m}_{injected} = 1.0$ kg/h. Air-injection yields to an increase in the axial velocity and changes the circumferential velocity component w from nearly zero for the undisturbed flow to w $\approx$ 10 m/s maximal. Obviously, swirl is produced within the tube but the velocity distribution is not entirely point-symmetric in respect to the centre. The vortex rotates anticlockwise around the x-axis.

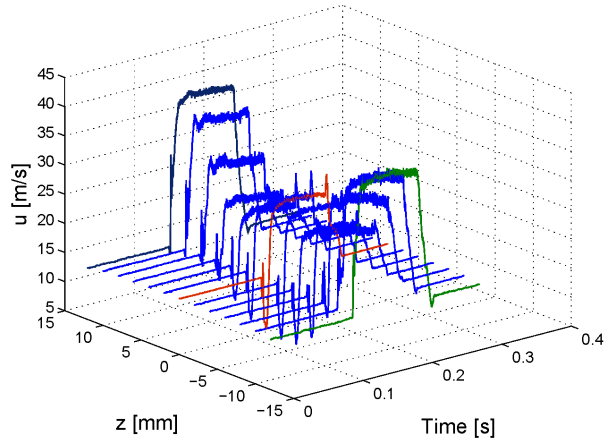

Figure 2: Change in the axial velocity u due to the circumferential air-injection into a swirl free tube flow with the VWG-Module 1. $M_{nozzle} = 1.0$ and $\dot{m}_{injected} = 1$ kg/h

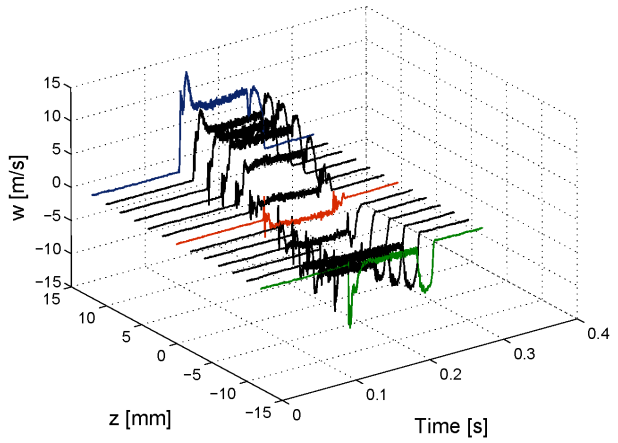

Figure 3: Change in the circumferential velocity w due to the circumferential air-injection into a swirl free tube flow with the VWG-Module 1. $M_{nozzle} = 1.0$ and $\dot{m}_{injected} = 1$ kg/h

In Figures 2-5 the velocities on the centreline are highlighted in red and near the tube walls they are labelled in green or dark blue.

4.2 Velocity changes due to air-injection into a swirling tube flow

The induced velocity changes due to the air-injection into the swirling tube flow are displayed in Figure 4 and 5. In this case VWG-Module 2 was used, the nozzle was choked and the injected mass flow rate amounted to $\dot{m}_{injected} = 1.0$ kg/h. The swirl intensity S was adjusted via the axial ($\dot{m}_a$) and circumferential ($\dot{m}_c$) mass flow rate to $S = \dot{m}_c/\dot{m}_a = 0.5$. The velocity components over the tube cross section in z-direction were selected for both Figures. Air-injection increases the anticlockwise rotating swirl of the mean flow in connection with an augmentation of the axial and circumferential velocity. The generated changes in the velocity profile are not point-symmetric. The maximum change in the velocity w does not occur on the tube circumference but between centreline and inner tube wall. The turbulence induced velocity fluctuations of the swirling flow with and without the temporary air-injection are higher than in Figure 2 and 3. Phase-averaging a turbulence influenced velocity signal minimises only the uncorrelated velocity fluctuations whereas the correlated ones remains in the signal.

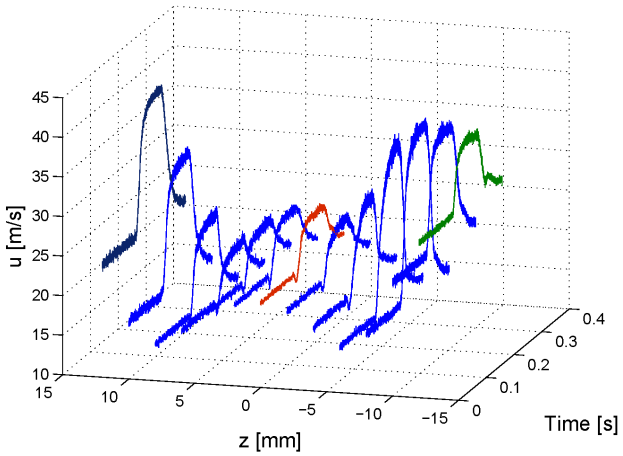

Figure 4: Change in the axial velocity u due to the air-injection into a swirling tube flow with the VWG-Module 2. Swirl intensity of the flow $S = \dot{m}_c/\dot{m}_a = 0.5$, $M_{nozzle} = 1.0$, and $\dot{m}_{injected} = 1$ kg/h

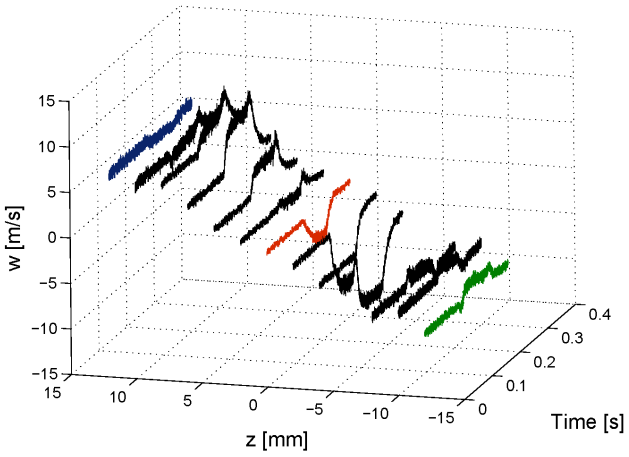

Figure 5: Change in the circumferential velocity w due to the air-injection into a swirling tube flow with the VWG-Module 2. Swirl intensity of the flow $S = \dot{m}_c/\dot{m}_a = 0.5$, $M_{nozzle} = 1.0$, and $\dot{m}_{injected} = 1$ kg/h

4.3 Direct and indirect noise separation

The propagation of the vorticity fluctuation corresponds to the flow velocity in contrast to acoustic waves which prop-

agates with the speed of sound. With the variation of the distance between VWG-Module 1 and nozzle throat different propagation delays occur. Consequently, such distance variation allows the separation of direct and indirect sound and their identification within the time signals of the detected acoustic pressure.

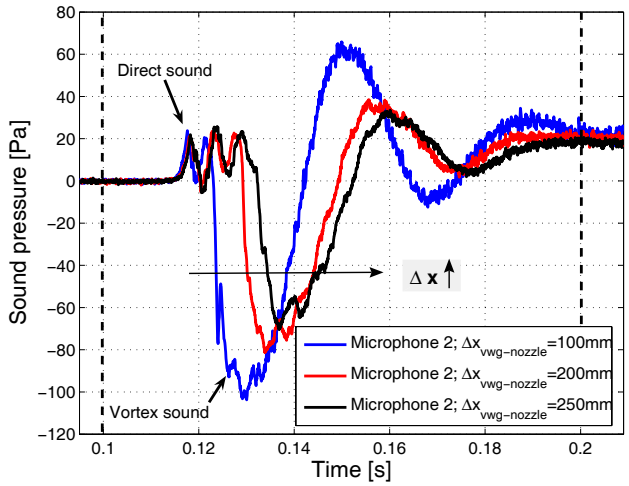

Figure 6: Acoustic pressure signals for distance variation between the VWG-Module 1 and the choked nozzle for the air-injection of $\dot{m}_{injected}$ = 1 kg/h

Figure 6 shows the acoustic pressure signals acquired at the microphone position 2 for three measurements conducted with tube sections of different lengths between the vortex module and the choked nozzle with an injected mass flow rate of $\dot{m}_{injected}$ = 1 kg/h. The leading and trailing edge of the trigger signal used to control the valve is indicated as dashed line. The direct sound peaks appear nearly at the same instant of time for each of the three test rig configurations, e.g. doubling the distance shifts the direct peak only by 0.28 ms. In contrast, the appearance of the negative pressure pulse is clearly delayed if the distance is augmented. The vorticity fluctuation generates a negative pressure pulse during its acceleration through the nozzle which propagates downstream as acoustic wave. The delay of the negative pressure pulse is related to the propagation path length between VWG-Module 1 and nozzle throat, and determines the occurrence in time of the generated indirect sound. As a result, distance augmentation increases the time delay of the appearing vortex sound. The simultaneous decay of the vortex sound amplitudes with increasing tube length is caused by the vortex energy decay occurring with the longer lasting vortex passage through the tube section upstream of the nozzle.

4.4 Vortex sound generation in swirl free and swirling tube flow

Beside the distance variation the generation of direct and vortex sound can also be visualised by varying the injected mass flow rate at a constant nozzle Mach number and for a constant distance between the VWG-Module and the nozzle.

In case of a choked nozzle and a fixed distance between each VWG-Module and the nozzle throat the air-injection into the swirl free and the swirling tube flow was increased and the changes in the time signals of the acoustic pressure were recorded. The acoustic pressure signals measured at

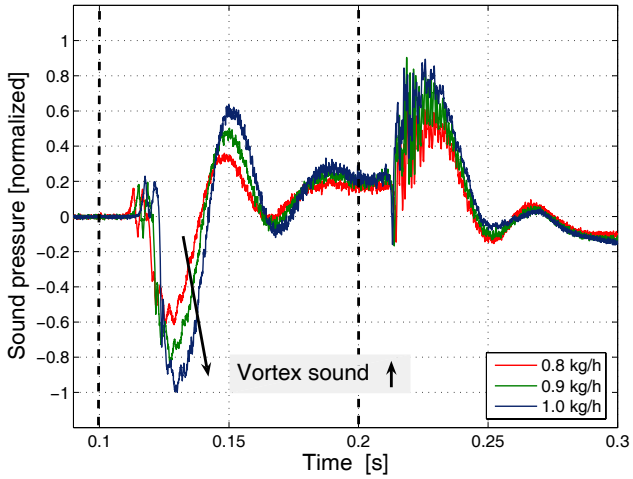

Figure 7: Vortex sound generated by various temporarily injected mass flow rates. Acoustic pressure signals at microphone position 2 using VWG-Module 1 and a choked nozzle with a fixed distance in between

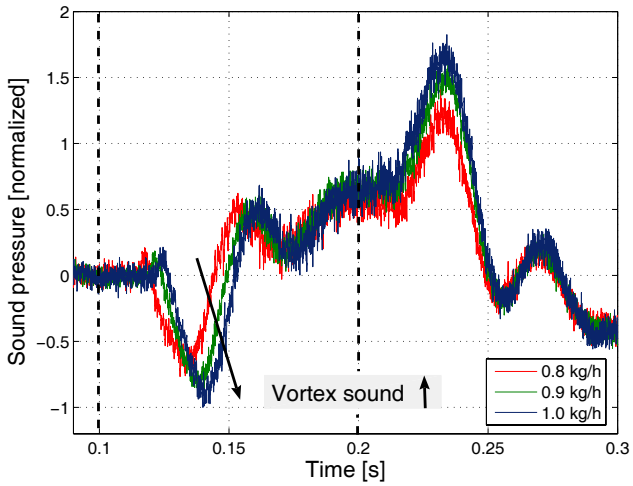

Figure 8: Vortex sound generated by various temporarily injected mass flow rates. Acoustic pressure signals at microphone position 2 using VWG-Module 2 and a choked nozzle with a fixed distance in between. Swirl intensity of the flow adjusted to $S = \dot{m}_c/\dot{m}_a = 0.5$

microphone position 2 are displayed in Figure 7 for the swirl free and in Figure 8 for the swirling tube flow. The trigger signal is indicated again as dashed lines. With the augmentation of the injected mass flow the generated indirect pressure pulse originated from the acceleration of the vorticity fluctuation increases. Besides, only small changes in the direct positive sound peak occur since the mechanical opening dominates the sound emission. The different time delays of the direct sound peaks relative to the leading edge of the trigger signal are caused by the pressure dependence on the opening of the fast-switching valve. In contrast, the valve closes nearly pressure independent at the same time.

Both acoustic pressure signals recorded for the swirl free and the swirling tube flow, are quite similar in spite of the higher noise component originated from the increased turbulence intensity in the swirling flow. In consequence, the generation of the negative pressure is not caused by the fluctuating mass flow itself when passing the choked nozzle since

this amount is identical in both cases. Instead, the temporary air-injection of a constant mass flow rate generates disturbances similar in shape but different in amplitude in the velocity/vorticity field for the swirl free and the swirling tube flow, see Figure 2-5. This results in different vortex sound amplitudes downstream as shown in the next section.

4.5 Vortex sound generation in swirling tube flows of various swirl intensities

In order to evaluate the influence of the swirl intensity within the swirling flow on the generated vortex sound, the mass flow rate in axial ($\dot{m}_a$) and circumferential direction ($\dot{m}_c$) was varied keeping the total mass flow constant. As parameter for the swirl intensity the ratio $S = \dot{m}_c/\dot{m}_a$ was used. Figure 9 shows the effect of the increased swirl intensity in the flow on the generated vortex sound in case of a choked nozzle. Therefore, the vortex sound amplitudes were extracted from the pressure signals recorded at microphone position 2 for various injected mass flow rates. The generated vortex sound increases for a constant injected mass flow rate with the augmentation of the intensity of the steady swirling flow.

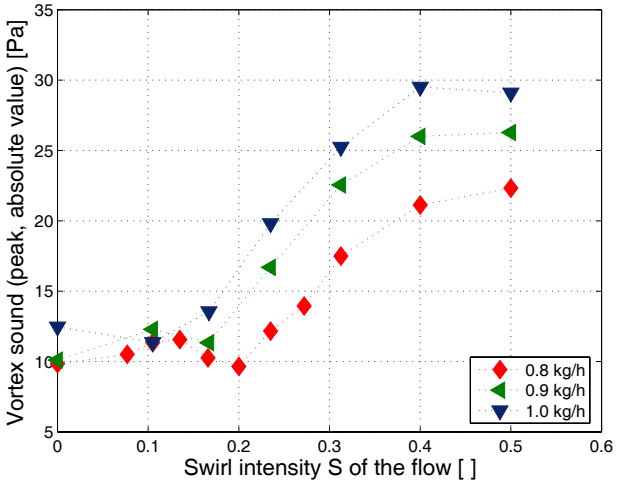

Figure 9: Vortex sound measured at microphone position 2 for various intensities of the swirling flow. Choked nozzle and fixed distance between VWG-Module 2 and nozzle

5 Conclusion

The generation of vortex sound due to the acceleration of artificially produced vorticity fluctuations was demonstrated in a model experiment. The vorticity alteration was realised within a swirl free and a swirling tube flow. The identification and separation of direct and indirect sound was achieved by varying the distance between VWG-Module 1 and nozzle throat. Air-injection yields to an unsteady swirling flow in the tube according to the injected mass flow rates. Increasing the air-injection either into the swirl free or the swirling flow augments the swirl upstream of the nozzle and the generated vortex sound. The produced sound through accelerated vorticity fluctuation increases with the intensity of the steady swirling flow. The shown results are the basis for future investigations concerning the vortex sound generation mechanism to figure out its relevance as an aero-engine noise source.

References

[1] F. Bake, C. Richter, B. Mühlbauer, N. Kings, I. Röhle, F. Thiele, B. Noll, "The entropy wave generator(EWG): A reference case on entropy noise", *J. Sound and Vibration* **326**, 574-598 (2009)

[2] H. Bruun, *Hot-Wire Anemometry*, Oxford University Press, Oxford (1995)

[3] N.A. Cumpsty, "Jet engine combustion noise: Pressure, entropy and vorticity perturbations produced by unsteady combustion or heat addition", *J. Sound and Vibration* **66**(4), 527-544 (1979)

[4] N.A. Cumpsty, F.E. Marble, "Core noise from gas turbine exhausts", *J. Sound and Vibration* **54**(2), 297-309 (1977)

[5] N.A. Cumpsty, F.E. Marble, "The interaction of entropy fluctuations with turbine blade rows; a mechanism of turbojet engine noise", *Proceedings of the Royal Society London A* **357**, 323-344 (1977)

[6] C.S. Gho, A.S. Morgans, "Phase prediction of the response of choked nozzles to entropy and acoustic disturbances", *J. Sound and Vibration* **330** (21), 5184-5198 (2011)

[7] M.S. Howe. *The Theory of Vortex Sound*, Cambridge University Press, Cambridge (2003)

[8] M.S. Howe, "Indirect combustion noise", *J. Fluid Mechanics* **659**, 267-288 (2010)

[9] S. Hulshoff, A. Hirschberg, G. Hofmans, "Sound production of vortex-nozzle interaction", *J. Fluid Mechanics* **439**, 335-352 (2001)

[10] F.E. Marble, S.M. Candel, "Acoustic disturbances from gas non-uniformities convected through a nozzle", *J. Sound and Vibration* **55**(2), 225-243 (1977)

[11] W. Moase, M. Brear, C. Manzie, "The forced response of choked nozzles and supersonic diffusers", *J. Fluid Mechanics* **585**, 281-304 (2007)

[12] C.L. Morfey, "Amplification of aerodynamic noise by convected flow inhomogeneities" *J. Sound and Vibration* **31** (4), 391-397 (1973)

[13] M. Leyko, S. Moreau, F. Nicoud, T. Poinsot, "Numerical and analytical modelling of entropy noise in a supersonic nozzle with shock", *J. Sound and Vibration* **330**, 3944-3958 (2011)

[14] S.R. Stow, A.P. Dowling, T.P. Hynes, "Reflection of circumferential modes in a choked nozzle", *J. Fluid Mechanics* **467** 215-239 (2002)